

RESEARCH ARTICLE

[View Article Online](#)  
[View Journal](#) | [View Issue](#)



Cite this: *Inorg. Chem. Front.*, 2024, 11, 4329

## Synergistic combination of different types of functional motif in $\text{Rb}(\text{NO}_3)(\text{SO}_3\text{NH}_3)$ for realizing excellent ultraviolet optical nonlinearity†

Yunxia Song,<sup>a</sup> Chensheng Lin, <sup>ID</sup><sup>b</sup> Xin Zhao,<sup>b</sup> Tao Yan, <sup>ID</sup><sup>b</sup> Ning Ye, <sup>ID</sup><sup>c</sup> Haotian Tian\*<sup>b</sup> and Min Luo <sup>ID</sup>\*<sup>b</sup>

The second harmonic generation (SHG) response, birefringence, and ultraviolet (UV) absorption edge are three crucial parameters of UV nonlinear optical (NLO) crystals. However, striking a balance among these parameters has been a challenging endeavor. The synergistic combination of mixed chromophores is regarded as an effective strategy to achieve this task, leveraging the benefits of both functional motifs. Herein, a novel UV NLO crystal,  $\text{Rb}(\text{NO}_3)(\text{SO}_3\text{NH}_3)$ , was successfully designed by integrating the  $\pi$ -conjugated  $[\text{NO}_3]$  unit with the non- $\pi$ -conjugated  $[\text{SO}_3\text{NH}_3]$  unit. As anticipated, the  $\pi$ -conjugated  $[\text{NO}_3]$  units contribute to a robust SHG effect and birefringence, while the non- $\pi$ -conjugated  $[\text{SO}_3\text{NH}_3]$  units help in widening the band gap and controlling the birefringence within an optimal range by decoupling the  $\pi$ -conjugated interactions and reducing the system's anisotropy. Consequently, it exhibits a strong SHG response (7  $\times$  KDP), moderate birefringence (0.07@546 nm), and a short UV absorption edge (208 nm), marking it as a promising UV NLO crystal.

Received 25th April 2024,  
Accepted 5th June 2024

DOI: 10.1039/d4qi01044b  
[rsc.li/frontiers-inorganic](http://rsc.li/frontiers-inorganic)

## Introduction

Ultraviolet (UV) nonlinear optical (NLO) crystals are vital components of solid-state lasers, holding substantial technical value in areas such as laser micro-machining and optical communication.<sup>1–4</sup> Consequently, the pursuit of novel UV NLO crystals has long been a focal point in the realms of laser and materials science.<sup>5–7</sup> Typically, a proficient UV NLO crystal should possess a short UV absorption edge (less than 300 nm), a potent second-harmonic generation (SHG) effect (greater than 5 times that of KDP), and a moderate birefringence (between 0.06 and 0.1).<sup>8,9</sup> However, achieving a balance among these three critical performances often proves challenging, resulting in a dearth of practical UV NLO crystals. Hence, the

design and synthesis of new UV NLO crystals with superior performance remains one of the most pressing challenges in the field.

Functional motif theory proposes that functional motifs serve as microstructural units, the composition and arrangement of which determine the properties of materials.<sup>10</sup> Typically, three critical properties of NLO crystals – the SHG effect, birefringence, and UV absorption edge – are intimately linked with three key parameters of the microscopic functional motifs: hyperpolarizability, polarizability anisotropy, and the HOMO–LUMO gap. At present,  $\pi$ -conjugated units and non- $\pi$ -conjugated units are frequently observed functional motifs in UV NLO crystals.<sup>11,12</sup> Notably,  $\pi$ -conjugated units like  $[\text{BO}_3]$ ,  $[\text{CO}_3]$ , and  $[\text{NO}_3]$  usually exhibit substantial hyperpolarizabilities and polarizability anisotropies, owing to their delocalized  $\pi$ -bonds.<sup>11</sup> Consequently, NLO materials with a  $\pi$ -conjugated system often demonstrate significant SHG effects and adequate birefringence. Nonetheless, it is crucial to note that the lower splitting energy of delocalized  $\pi$ -bonds means  $\pi$ -conjugated units tend to possess a smaller HOMO–LUMO gap than non- $\pi$ -conjugated units.<sup>11</sup> Furthermore, the large polarizability anisotropy can lead to excessive birefringence when the density of these  $\pi$ -conjugated units is high or coplanar, resulting in spatial walk-off effects that can significantly degrade the output beam quality.<sup>13</sup> A prime example of this is the commercially available  $\beta\text{-BaB}_2\text{O}_4$  (BBO) crystal. Despite its

<sup>a</sup>School of Electronic, Electrical Engineering and Physics, Fujian University of Technology, Fuzhou, Fujian, 350108, China

<sup>b</sup>Key Laboratory of Optoelectronic Materials Chemistry and Physics, Fujian Institute of Research on the Structure of Matter, Chinese Academy of Sciences, Fuzhou, Fujian 350002, China. E-mail: lm8901@fjirm.ac.cn, tianhaotian@fjirm.ac.cn

<sup>c</sup>Tianjin Key Laboratory of Functional Crystal Materials, Institute of Functional Crystal, Tianjin University of Technology, Tianjin, 300384, China

† Electronic supplementary information (ESI) available: Crystallographic and structure data (Tables S1–S4), and figures containing the measurement results and detail of  $\text{RbNO}_3\text{SO}_3\text{NH}_3$  (Fig. S1–S5). CCDC 2351069 for  $\text{RbNO}_3\text{SO}_3\text{NH}_3$ . For ESI and crystallographic data in CIF or other electronic format see DOI: <https://doi.org/10.1039/d4qi01044b>

excellent SHG efficiency ( $>5 \times$  KDP) and short UV absorption edge (189 nm), its excessive birefringence (0.113@1064 nm) severely limits its application in high-power output fields.<sup>14,15</sup> In contrast, non- $\pi$ -conjugated units, due to the absence of a delocalized  $\pi$ -bond, have a restricted electron delocalization range. This typically results in a larger HOMO-LUMO gap and smaller polarizability anisotropy and hyperpolarizability.<sup>16</sup> While a smaller polarization anisotropy can effectively prevent spatial walk-off effects, it also makes it challenging to generate adequate birefringence, thereby limiting the phase-matching wavelength range of the material.<sup>17</sup> Additionally, the reduced hyperpolarization of non- $\pi$  conjugated systems typically leads to a smaller SHG effect compared to  $\pi$  conjugated systems. As such, the challenge lies in expanding the band gap and maintaining birefringence within a suitable range while ensuring a sufficient SHG effect – a difficult yet meaningful endeavor.

Based on the above ideas, we hope to design high-performance UV NLO materials by combining  $\pi$  conjugated and non- $\pi$  conjugated units, including the following three considerations: (i) the substantial hyperpolarization and polarizability anisotropy of the  $\pi$ -conjugated unit can yield significant SHG effects and birefringence; (ii) the relatively lower polarizability anisotropy of the non- $\pi$ -conjugated units could potentially reduce the system's anisotropy, thereby preventing the generation of excessive birefringence; (iii) as per a prior study by Chen *et al.*, non- $\pi$ -conjugated units can partially isolate the  $\pi$ -conjugated interactions through  $\pi$ -conjugation confinement, which could potentially facilitate bandgap expansion.

In the current study, we opted for the triangular  $\pi$ -conjugated  $[\text{NO}_3]$  unit in conjunction with our previously identified polar tetrahedral non- $\pi$ -conjugated  $[\text{SO}_3\text{NH}_3]$  unit. The  $[\text{NO}_3]$  unit demonstrates a stronger hyperpolarizability and polarizability anisotropy compared to other triangular  $\pi$ -conjugated units such as  $[\text{CO}_3]$  and  $[\text{BO}_3]$  units. Conversely, the  $[\text{SO}_3\text{NH}_3]$  unit possesses a considerable HOMO-LUMO gap and can further amplify hyperpolarizability through hydrogen-bonding interactions with the  $[\text{NO}_3]$  unit. In addition, as alkali metal ions lack d-d and f-f transitions, they are more favorable for UV light transmission. Consequently, Rb cations were selected as counterions to maintain charge equilibrium. As a result of this approach, we successfully synthesized a novel UV NLO crystal,  $\text{Rb}(\text{NO}_3)(\text{SO}_3\text{NH}_3)$ , which displays a substantial SHG effect ( $7 \times$  KDP), moderate birefringence (0.07@546 nm), and a short UV absorption edge (208 nm).

## Experimental section

### Reagents

$\text{RbNO}_3$  (Adamas, 99.0%),  $\text{SO}_3\text{NH}_3$  (Adamas, 99.0%).

### Synthesis

$\text{RbNO}_3$  and  $\text{SO}_3\text{NH}_3$  were dissolved in 5 ml  $\text{H}_2\text{O}$  and evaporated in an oven at 55 °C. After 3 days,  $\text{RbNO}_3\text{SO}_3\text{NH}_3$  crystals were obtained.

### Single-crystal X-ray diffraction

The crystal structure of  $\text{RbNO}_3\text{SO}_3\text{NH}_3$  was determined using SC-XRD data collected with a Rigaku Mercury CCD diffractometer and graphite-monochromated Mo-K $\alpha$  radiation ( $\lambda = 0.7103 \text{ \AA}$ ). The structure was solved using ShelXT and refined with ShelXL on the OLEX2 package.<sup>18</sup> Table S1† shows the crystallographic data and structure refinements for  $\text{RbNO}_3\text{SO}_3\text{NH}_3$ . Tables S2–S4† display the atomic coordinates, equivalent isotropic displacement parameters, selected bond lengths and angles, and anisotropic displacement parameters for  $\text{RbNO}_3\text{SO}_3\text{NH}_3$ .

### Power X-ray diffraction

The PXRD data of  $\text{RbNO}_3\text{SO}_3\text{NH}_3$  were obtained using a Miniflex600 instrument with Cu K $\alpha$  radiation ( $\lambda = 1.540598 \text{ \AA}$ ) in the  $2\theta$  range from 5 to 60°.

### Energy-dispersive X-ray spectroscopy analysis

Microprobe elemental analyses were recorded on a field emission scanning electron microscope (FESEM, SU-8010) with an energy dispersive X-ray spectrometer (EDS).

### Thermal analysis

Thermogravimetric analysis (TGA) was conducted using a Netzsch STA449F3 simultaneous analyzer under flowing  $\text{N}_2$  at a rate of 10 °C min<sup>-1</sup>.

### UV-Vis diffuse reflectance spectroscopy

The diffuse reflectance spectrum of  $\text{RbNO}_3\text{SO}_3\text{NH}_3$  was measured using a PerkinElmer Lamda950 UV/vis/NIR spectrophotometer, with  $\text{BaSO}_4$  as the standard.

### Birefringence measurement

The polarizing microscope was used to measure the birefringence of  $\text{RbNO}_3\text{SO}_3\text{NH}_3$  with 546.1 nm light. The birefringence was calculated using the following formula:

$$R = (|N_e - N_o|) \times T = \Delta n \times T \quad (\text{S1})$$

$R$  denotes optical path difference,  $\Delta n$  represents birefringence, and  $T$  is the thickness of the crystal.

### Second harmonic generation measurements

The polycrystalline SHG signals for  $\text{RbNO}_3\text{SO}_3\text{NH}_3$  were measured on a 1064 nm solid-state laser with KDP crystals as reference samples. The crystals were ground and sieved into six different sizes: 25–45  $\mu\text{m}$ , 45–62  $\mu\text{m}$ , 62–75  $\mu\text{m}$ , 75–109  $\mu\text{m}$ , 109–150  $\mu\text{m}$ , and 150–212  $\mu\text{m}$ .

### Theoretical calculations

Density functional theory (DFT) was used to calculate the band structure of  $\text{RbNO}_3\text{SO}_3\text{NH}_3$ .<sup>19</sup> The exchange–correlation energy was treated by the generalized gradient approximation (GGA) with the Perdew–Burke–Ernzerhof (PBE) functional.<sup>20</sup> The valence electrons for the following atoms are Li 2s<sup>1</sup>; C 2s<sup>2</sup> 2p<sup>2</sup>; O 2s<sup>2</sup> 2p<sup>4</sup>; N 2s<sup>2</sup> 2p<sup>3</sup>; and H 1s<sup>1</sup>. The energy cutoff for

$\text{RbNO}_3\text{SO}_3\text{NH}_3$  was set at 600 eV, and the Monkhorst–Pack grid size was  $2 \times 2 \times 2$ .<sup>21</sup> The HSE06 functional was used to calculate the band gap and densities of states (DOS) for  $\text{RbNO}_3\text{SO}_3\text{NH}_3$ .<sup>22</sup> The NLO coefficient  $d_{ij}$  was calculated by using an expression originally proposed by Rashkeev *et al.* and developed by Lin *et al.*<sup>23</sup>

## Results and discussion

$\text{RbNO}_3\text{SO}_3\text{NH}_3$  crystallized in the non-centrosymmetric (NCS) space group  $Pmc2_1$  (no. 26) of the orthorhombic crystal system with lattice parameters  $a = 5.6303(3)$  Å,  $b = 7.4552(5)$  Å, and  $c = 8.0537(5)$  Å. In the structure, each N atom is coordinated with three O atoms to form the triangular unit  $[\text{NO}_3]$  (Fig. 1a), and each S atom is coordinated with one  $\text{NH}_3$  and three O atoms to form the polar tetrahedral unit  $[\text{SO}_3\text{NH}_3]$  (Fig. 1b). The  $[\text{SO}_3\text{NH}_3]$  unit and the  $[\text{NO}_3]$  unit are connected by hydrogen bonds to form a  $[\text{NO}_3\text{SO}_3\text{NH}_3]$  one-dimensional polar chain, in which  $[\text{SO}_3\text{NH}_3]$  and  $[\text{NO}_3]$  units are distributed alternately (Fig. 1c). These one-dimensional polar chains are further connected by Rb ions and extended along the  $b$  and  $c$  directions, resulting in the 3D structure of  $\text{RbNO}_3\text{SO}_3\text{NH}_3$  (Fig. 1d). In the structure, the dipole moments of each one-dimensional chain are superimposed along the  $c$ -direction within the constraints of the  $\text{RbO}_9$  polyhedra, which may contribute to the strong SHG response (Fig. 1e).

$\text{RbNO}_3\text{SO}_3\text{NH}_3$  was synthesized *via* the aqueous solution method. PXRD confirmed the purity of the crystals (Fig. S1†), while EDS confirmed that the crystals were composed of Rb, O, N, and S elements (Fig. S2†). Thermal analysis indicated that  $\text{RbNO}_3\text{SO}_3\text{NH}_3$  remained stable up to 127 °C (Fig. S3†).

Diffuse reflectance spectroscopy showed that the UV absorption edge is about 208 nm, corresponding to a bandgap of 5.96 eV (Fig. 2a). HSE06 calculations showed that  $\text{RbNO}_3\text{SO}_3\text{NH}_3$  has a direct band gap of 5.657 eV (Fig. 2b), matching closely with the measured value. Such a wide bandgap is significantly larger than that of  $\text{RbNO}_3$  (5.251 eV). As described above, this may be because  $[\text{SO}_3\text{NH}_3]$  units intercept the delocalized  $\pi$ – $\pi$  interactions between  $[\text{NO}_3]$  units, and thus enlarge the band gap. To confirm this inference, the PDOS of  $\text{RbNO}_3$  and  $\text{RbNO}_3\text{SO}_3\text{NH}_3$  were calculated, respectively (Fig. S4†). One can find that the conduction band minimum (CBM) of  $\text{RbNO}_3\text{SO}_3\text{NH}_3$  is occupied by N 2p and O 2p orbitals. Compared to  $\text{RbNO}_3$ , the N–O  $\pi^*$ – $\pi^*$  component of the CBM in  $\text{RbNO}_3\text{SO}_3\text{NH}_3$  is significantly lower, and thus pulls up the bottom of the CB.

The SHG effect of  $\text{RbNO}_3\text{SO}_3\text{NH}_3$  was tested based on the Kurtz–Perry method,<sup>24</sup> with KDP as the standard. The results showed that  $\text{RbNO}_3\text{SO}_3\text{NH}_3$  exhibited phase-matched behavior and SHG effects up to 7 × KDP (Fig. 2c). According to the formula  $d_{\text{eff}} = d_{\text{eff}, \text{KDP}} (I_{2\omega, \text{sample}}/I_{2\omega, \text{KDP}})^{1/2}$  ( $d_{\text{eff}, \text{KDP}} = 0.26 \text{ pm V}^{-1}$ ),<sup>25,26</sup> the effective SHG coefficient  $d_{\text{eff}}$  of  $\text{RbNO}_3\text{SO}_3\text{NH}_3$  was 1.82 pm V<sup>-1</sup>. In addition, the calculated

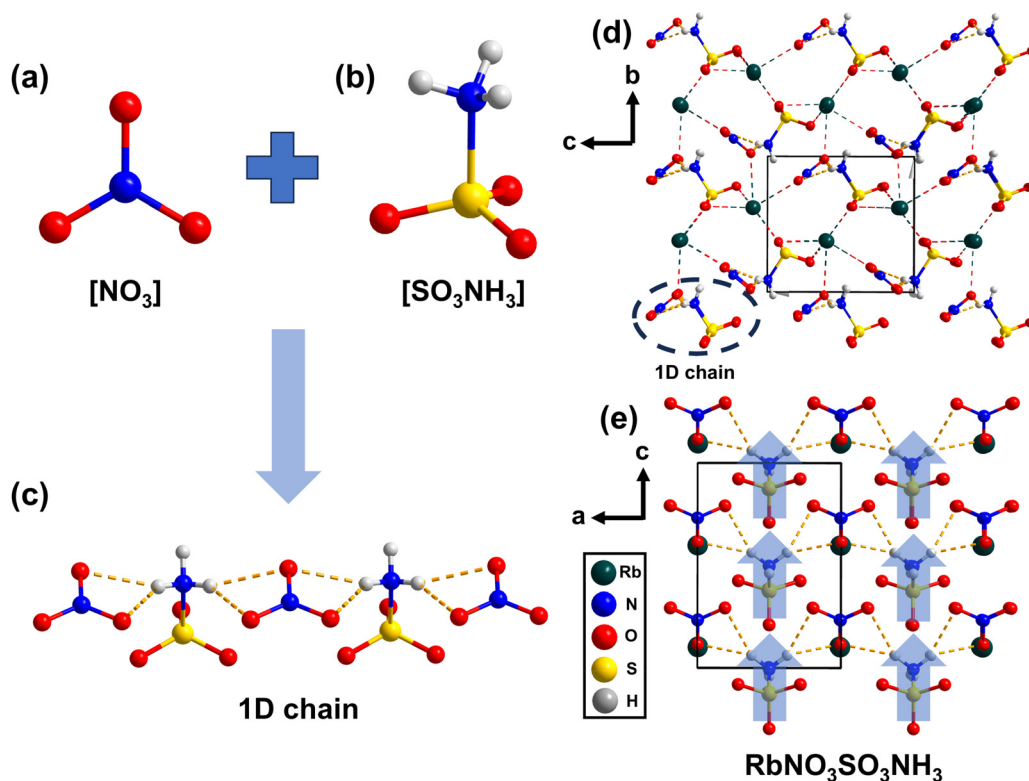


**Fig. 1** (a)  $[\text{NO}_3]$  unit. (b)  $[\text{SO}_3\text{NH}_3]$  unit. (c)  $[\text{NO}_3\text{SO}_3\text{NH}_3]$  one-dimensional polar chain. 3D crystal structure of  $\text{RbNO}_3\text{SO}_3\text{NH}_3$  (d) in the  $b$ – $c$  plane and (e) in the  $a$ – $c$  plane.

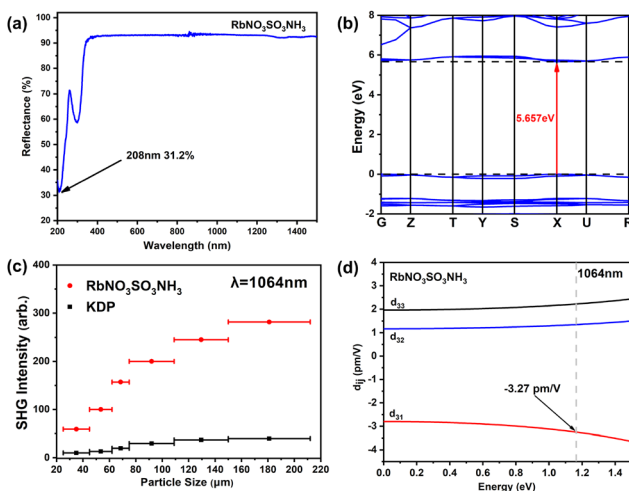


**Fig. 2** (a) UV/Vis diffuse-reflectance spectrum of  $\text{RbNO}_3\text{SO}_3\text{NH}_3$ ; (b) calculated electronic band structures for  $\text{RbNO}_3\text{SO}_3\text{NH}_3$  based on HSE06; (c) power SHG measurement at 1064 nm; (d) calculated SHG coefficients of  $\text{RbNO}_3\text{SO}_3\text{NH}_3$ .

maximum SHG coefficient  $d_{31}$  was  $-3.27 \text{ pm V}^{-1}$  (Fig. 2d), which is consistent with the experimental values. According to functional motif theory, the SHG effect of  $\text{RbNO}_3\text{SO}_3\text{NH}_3$  should be contributed by the functional motif  $[\text{NO}_3]$  and  $[\text{SO}_3\text{NH}_3]$  units. Based on the anion group theory,<sup>27</sup> the SHG contribution of the  $[\text{NO}_3]$  unit is directly proportional to its number density ( $n\text{V}^{-1}$ ) and structural criterion ( $C$ ), while the SHG contribution of the  $[\text{SO}_3\text{NH}_3]$  unit is proportional to its dipole moment per unit volume. For  $\text{RbNO}_3\text{SO}_3\text{NH}_3$ , the number density ( $n\text{V}^{-1}$ ) and the structural criterion ( $C$ ) of the  $[\text{NO}_3]$  unit are 0.0059 and 0.7702, respectively, and the dipole moments per unit volume are  $0.022 \text{ D } \text{\AA}^{-3}$ . These values are all comparable to those we previously reported for  $\text{KNO}_3\text{SO}_3\text{NH}_3$ ,<sup>28</sup> and thus should be the main reason for the large SHG effects. In addition, according to our previous study, hydrogen bonding between the  $[\text{SO}_3\text{NH}_3]$  unit and  $[\text{NO}_3]$  unit can change the electron distribution in the  $\pi$ -orbital, which can further enhance the SHG effect. The hyperpolarization of the  $[\text{SO}_3\text{NH}_3\text{NO}_3]$  unit in the structure is 147, significantly higher than the sum of the hyperpolarization of the  $[\text{SO}_3\text{NH}_3]$  unit and the  $[\text{NO}_3]$  unit. This confirms that the hydrogen-bonding interactions between the  $[\text{SO}_3\text{NH}_3]$  unit and  $[\text{NO}_3]$  unit also contribute to the formation of large SHG effects. Interestingly, although the number density ( $n\text{V}^{-1}$ ) and structural criterion ( $C$ ) of  $[\text{NO}_3]$  units, as well as the dipole moments per unit volume of  $[\text{SO}_3\text{NH}_3]$  units in  $\text{RbNO}_3\text{SO}_3\text{NH}_3$ , are comparable to those previously reported for  $\text{KNO}_3\text{SO}_3\text{NH}_3$ , the hyperpolarization of  $[\text{SO}_3\text{NH}_3\text{NO}_3]$  units in  $\text{RbNO}_3\text{SO}_3\text{NH}_3$  is greater than that in  $\text{KNO}_3\text{SO}_3\text{NH}_3$ . However,  $\text{RbNO}_3\text{SO}_3\text{NH}_3$  exhibits a smaller SHG effect than  $\text{KNO}_3\text{SO}_3\text{NH}_3$ . To elucidate the microscopic mechanism behind this SHG difference, the SHG weighted electron density was calculated. As shown in Fig. S5,† the maximum tensor  $d_{31}$  of  $\text{RbNO}_3\text{SO}_3\text{NH}_3$  and the maximum tensor  $d_{21}$  of  $\text{KNO}_3\text{SO}_3\text{NH}_3$  indeed are both contributed by the

$[\text{NO}_3]$  units and the  $[\text{SO}_3\text{NH}_3]$  units. However, the contribution of the  $[\text{NO}_3]$  unit to  $\text{RbNO}_3\text{SO}_3\text{NH}_3$  is significantly less than its contribution to  $\text{KNO}_3\text{SO}_3\text{NH}_3$ . As a result, the maximum tensor  $d_{31}$  of  $\text{RbNO}_3\text{SO}_3\text{NH}_3$  is significantly smaller than that of  $\text{KNO}_3\text{SO}_3\text{NH}_3$ , which may be the main reason for the SHG effect difference. In addition, since Rb ions possess a greater electron density around them than is around K ions,  $\text{RbNO}_3\text{SO}_3\text{NH}_3$  possesses a higher refractive index than  $\text{KNO}_3\text{SO}_3\text{NH}_3$  (Fig. 3c). This difference in refractive index may cause the 532 nm laser light to have a different phase-matching angle in the two crystals, which may also be one of the reasons for the SHG effect difference.

The birefringence of  $\text{RbNO}_3\text{SO}_3\text{NH}_3$  was tested using a polarized light microscope. The results indicate that the birefringence of  $\text{RbNO}_3\text{SO}_3\text{NH}_3$  at 546.1 nm is 0.07 (Fig. 3a and b), which is consistent with the theoretical calculations (Fig. 3c). It is noteworthy that this value is significantly higher than that of most NLO materials that only contain non- $\pi$  conjugated functional motifs, such as  $\text{KH}_2\text{PO}_4$  (0.035@1064 nm),<sup>29</sup>  $\text{Ba}_3\text{P}_3\text{O}_{10}\text{Cl}$  (0.03@1064 nm),<sup>30</sup>  $\text{K}_4\text{Mg}_4(\text{P}_2\text{O}_7)_3$  (0.0108@1064 nm),<sup>31</sup>  $\text{Li}_2\text{SO}_4\text{H}_2\text{O}$  (0.023@1064 nm),<sup>32</sup>  $\text{La}(\text{NH}_4)(\text{SO}_4)_2$  (0.03@1064 nm),<sup>33</sup>  $\text{NaNH}_4\text{PO}_3\text{F}\cdot\text{H}_2\text{O}$  (0.053@589.3 nm),<sup>34</sup>  $\text{Sr}(\text{NH}_2\text{SO}_3)_2$  (0.056@589.3 nm),<sup>35</sup>  $\text{Ba}(\text{NH}_2\text{SO}_3)_2$  (0.028@546.1 nm),<sup>35</sup> and  $\text{Ba}(\text{SO}_3\text{CH}_3)_2$  (0.04@589.3 nm). In addition, compared with most nitrate NLO materials, such as  $\text{Pb}_2(\text{NO}_3)_2(\text{H}_2\text{O})\text{F}_2$  (0.230@1064 nm),<sup>36</sup>  $\text{Sc}(\text{IO}_3)_2(\text{NO}_3)$  (0.348@546 nm),<sup>37</sup>  $\text{Pb}_2(\text{BO}_3)(\text{NO}_3)$  (0.174@1064 nm),<sup>38</sup> and  $\text{Cs}_2\text{Pb}(\text{NO}_3)_2\text{Br}_2$  (0.147@546 nm),<sup>39</sup>  $\text{RbNO}_3\text{SO}_3\text{NH}_3$  has a more suitable birefringence, which is equivalent to that of KBBF (0.077@546 nm).<sup>40</sup> In general, the optical properties of a crystal are determined by the electronic states near the forbidden band. As shown in Fig. S4,† the vicinity of the forbidden band of the title compound is occupied by the N-p and O-p states, indicating that its birefringence is entirely contributed by the  $[\text{NO}_3]$  units. On the one hand, this may be due to the large polarizability anisotropy of the  $[\text{NO}_3]$  unit preventing the too-small birefringence, and on the other hand, according to our previous study,<sup>41,42</sup> this noncoplanar arrangement of  $\pi$ -conjugated units can effectively avoid the overlarge birefringence. These factors may be the main reasons for the moderate birefringence of the title compound. Further, the calculated refractive index dispersion curves indicate that the

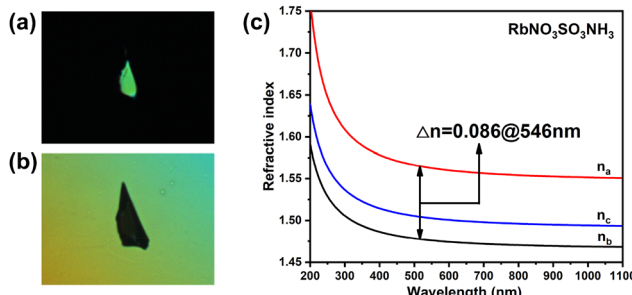


**Fig. 3** (a) Single crystal of  $\text{RbNO}_3\text{SO}_3\text{NH}_3$  under the polarizing microscope; (b)  $\text{RbNO}_3\text{SO}_3\text{NH}_3$  crystal achieves complete extinction under the compensator; (c) the calculated refractive indices of  $\text{RbNO}_3\text{SO}_3\text{NH}_3$ .

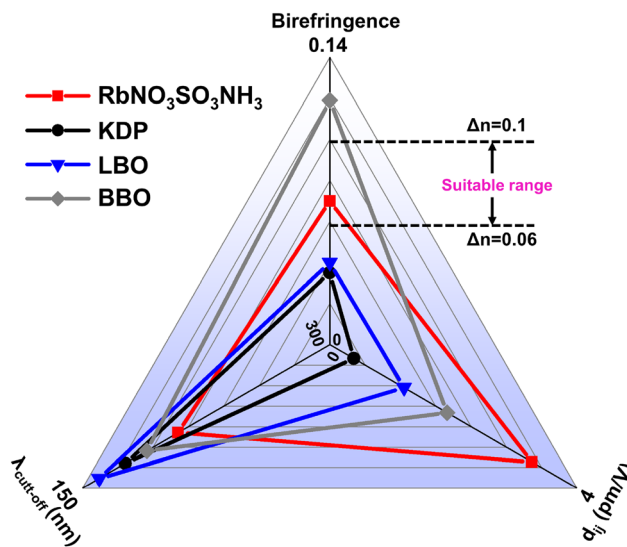


Fig. 4 Radar chart (there are three directions in the radar chart, which represent the ultraviolet absorption edge, maximum SHG coefficient, and birefringence, respectively).

birefringence of RbNO<sub>3</sub>SO<sub>3</sub>NH<sub>3</sub> is 0.086@546 nm, which is basically in agreement with the experimental results.

To evaluate the comprehensive performance of RbNO<sub>3</sub>SO<sub>3</sub>NH<sub>3</sub>, radargrams were plotted while commercial UV-NLO crystals KDP, LBO and BBO were used for comparison. As shown in Fig. 4, RbNO<sub>3</sub>SO<sub>3</sub>NH<sub>3</sub> displays larger SHG coefficients than KDP, BBO, and LBO, while also maintaining a short UV absorption edge. More importantly, it has more suitable birefringence, which not only contributes to the phase-matching performance of the material in the UV region but also can effectively prevent the occurrence of the walk-away effect. Overall, RbNO<sub>3</sub>SO<sub>3</sub>NH<sub>3</sub> achieves a balance between strong SHG effects, moderate birefringence, and short UV absorption edges, making it a promising UV NLO material.

## Conclusions

In summary, a novel UV NLO material, Rb(NO<sub>3</sub>)(SO<sub>3</sub>NH<sub>3</sub>), has been successfully synthesized through the integration of [NO<sub>3</sub>] and [SO<sub>3</sub>NH<sub>3</sub>] units. The synergistic interaction between these units contributes to a potent SHG response (7 × KDP). In addition, the one-dimensional chain structure composed of [NO<sub>3</sub>] and [SO<sub>3</sub>NH<sub>3</sub>] units, coupled with the reduction of system anisotropy by the [SO<sub>3</sub>NH<sub>3</sub>] units, engenders suitable birefringence (0.07@546 nm). Meanwhile, due to the spaced arrangement of [NO<sub>3</sub>] and [SO<sub>3</sub>NH<sub>3</sub>] units in the chain, the  $\pi$ -conjugated interactions between [NO<sub>3</sub>] units are decoupled by the [SO<sub>3</sub>NH<sub>3</sub>] units, resulting in its short UV absorption edge of 208 nm. Consequently, Rb(NO<sub>3</sub>)(SO<sub>3</sub>NH<sub>3</sub>) strikes a balance among three key properties, marking it as a promising UV NLO crystal.

## Conflicts of interest

There are no conflicts to declare.

## Acknowledgements

This work was supported by the National Natural Science Foundation of China (22305038, 22222510) and the Natural Science Foundation of Fujian Province (2021J011080).

## References

- 1 N. Savage, Ultraviolet lasers, *Nat. Photonics*, 2007, **1**, 83–85.
- 2 D. Cyranoski, China's crystal cache: a Chinese laboratory is the only source of a valuable crystal. David Cyranoski investigates why it won't share its supplies, *Nature*, 2009, **457**, 953–955.
- 3 F. Xu, G. Zhang, M. Luo, G. Peng, Y. Chen, T. Yan and N. Ye, A powder method for the high-efficacy evaluation of electro-optic crystals, *Natl. Sci. Rev.*, 2021, **8**, nwaa104.
- 4 D. F. Eaton, Nonlinear Optical Materials, *Science*, 1991, **253**, 281–287.
- 5 G. H. Zou and K. M. Ok, Novel ultraviolet (UV) nonlinear optical (NLO) materials discovered by chemical substitution-oriented design, *Chem. Sci.*, 2020, **11**, 5404–5409.
- 6 X. H. Dong, H. B. Huang, L. Huang, Y. Q. Zhou, B. B. Zhang, H. M. Zeng, Z. E. Lin and G. H. Zou, Unearthing Superior Inorganic UV Second-Order Nonlinear Optical Materials: A Mineral-Inspired Method Integrating First-Principles High-Throughput Screening and Crystal Engineering, *Angew. Chem., Int. Ed.*, 2024, **63**, e202318976.
- 7 Q. Liu, C. Hu, X. Su, M. Abudoureheman, S. L. Pan and Z. H. Yang, LiGeBO<sub>4</sub>: a nonlinear optical material with a balance between deep-ultraviolet cut-off edge and large SHG response induced by hand-in-hand tetrahedra, *Inorg. Chem. Front.*, 2019, **6**, 914–919.
- 8 H. X. Fan, N. Ye and M. Luo, New Functional Groups Design toward High Performance Ultraviolet Nonlinear Optical Materials, *Acc. Chem. Res.*, 2023, **56**, 3099–3109.
- 9 L. L. Wu, C. S. Lin, H. T. Tian, Y. Q. Zhou, H. X. Fan, S. D. Yang, N. Ye and M. Luo, Mg(C<sub>3</sub>O<sub>4</sub>H<sub>2</sub>)(H<sub>2</sub>O)<sub>2</sub>: A New Ultraviolet Nonlinear Optical Material Derived from KBe<sub>2</sub>BO<sub>3</sub>F<sub>2</sub> with High Performance and Excellent Water-Resistance, *Angew. Chem., Int. Ed.*, 2024, **63**, e202315647.
- 10 X. M. Jiang, S. Deng, M. H. Whangbo and G. C. Guo, Material Research from the Viewpoint of Functional Motifs, *Natl. Sci. Rev.*, 2022, **9**, nwac017.
- 11 L. Xiong, L. M. Wu and L. Chen, A General Principle for DUV NLO Materials: p-Conjugated Confinement Enlarges Band Gap, *Angew. Chem., Int. Ed.*, 2021, **60**, 25063–25067.
- 12 H. T. Qiu, F. M. Li, C. C. Jin, Z. H. Yang, J. J. Li, S. L. Pan and M. R. D. Mutailipu, Fluorination Strategy Towards Symmetry Breaking of Boron-centered Tetrahedron for

Poly-fluorinated Optical Crystals, *Angew. Chem., Int. Ed.*, 2024, **63**, e20231619.

13 X. H. Meng, X. Y. Zhang, Q. X. Liu, Z. Y. Zhou, X. X. Jiang, Y. G. Wang, Z. S. Lin and M. J. Xia, Nonlinear Optical Materials Perfectly Encoding  $\pi$ -Conjugated Anions in the  $\text{RE}_5(\text{C}_3\text{N}_3\text{O}_3)_2(\text{OH})_{12}$  ( $\text{RE} = \text{Y, Yb, Lu}$ ) Family with Strong Second Harmonic Generation Response and Balanced Birefringence, *Angew. Chem., Int. Ed.*, 2022, e202214848.

14 C. T. Chen, Y. B. Wang, B. C. Wu, K. C. Wu, W. L. Zeng and L. H. Yu, Design and synthesis of an ultraviolet-transparent nonlinear optical crystal  $\text{Sr}_2\text{Be}_2\text{B}_2\text{O}_7$ , *Nature*, 1995, **373**, 322–324.

15 L. L. Cao, H. T. Tian, D. H. Lin, C. S. Lin, F. Xu, Y. L. Han, T. Yan, J. D. Chen, B. X. Li, N. Ye and M. Luo, A flexible functional module to regulate ultraviolet optical nonlinearity for achieving a balance between a second-harmonic generation response and birefringence, *Chem. Sci.*, 2022, **13**, 6990.

16 H. T. Tian, C. S. Lin, X. Zhao, F. Xu, C. Wang, N. Ye and M. Luo,  $\text{Ba}(\text{SO}_3\text{CH}_3)_2$ : A Deep-Ultraviolet Transparent Crystal with Excellent Optical Nonlinearity Based on a New Polar Non- $\pi$ -Conjugated NLO Building Unit  $\text{SO}_3\text{CH}_3^-$ , *CCS Chem.*, 2023, **5**, 2497–2505.

17 H. T. Tian, N. Ye and M. Luo, Sulfamide: A Promising Deep-Ultraviolet Nonlinear Optical Crystal Assembled from Polar Covalent  $[\text{SO}_2(\text{NH}_2)_2]$  Tetrahedra, *Angew. Chem., Int. Ed.*, 2022, **61**, e202200395.

18 G. M. Sheldrick, A short history of SHELX, *Acta Crystallogr.*, 2008, **64**, 112–122.

19 W. Kohn, Nobel Lecture: Electronic structure of matter-wave functions and density functionals, *Rev. Mod. Phys.*, 1999, **71**, 1253–1266.

20 J. P. Perdew, K. Burke and M. Ernzerhof, Generalized Gradient Approximation Made Simple, *Phys. Rev. Lett.*, 1996, **77**, 3865.

21 H. J. Monkhorst and J. D. Pack, Special points for Brillouin-zone integrations, *Phys. Rev. B: Solid State*, 1976, **13**, 5188–5192.

22 L. Kang, S. Y. Luo, H. W. Huang, N. Ye, Z. S. Lin, J. G. Qin and C. T. Chen, Prospects for Fluoride Carbonate Nonlinear Optical Crystals in the UV and Deep-UV Regions, *J. Phys. Chem. C*, 2013, **117**, 25684–25692.

23 J. Lin, M. H. Lee, Z. P. Liu, C. T. Chen and C. J. Pickard, Mechanism for linear and nonlinear optical effects in beta- $\text{BaB}_2\text{O}_4$  crystals, *Phys. Rev. B: Condens. Matter Mater. Phys.*, 1999, **60**, 13380.

24 S. K. Kurtz and T. T. Perry, A power technique for evaluation of nonlinear optical materials, *J. Appl. Phys.*, 1968, **39**, 3798–3813.

25 W. F. Chen, B. W. Liu, S. M. Pei, X. M. Jiang and G. C. Guo,  $[\text{K}_2\text{PbX}][\text{Ga}_7\text{S}_{12}]$  ( $\text{X} = \text{Cl, Br, I}$ ): The First Lead-Containing Cationic Moieties with Ultrahigh Second-Harmonic Generation and Band Gaps Exceeding the Criterion of 2.33 eV, *Adv. Sci.*, 2023, **10**, 2207630.

26 D. Eimerl, Electro-optic, linear, and nonlinear optical properties of KDP and its isomorphs, *Ferroelectrics*, 1987, **72**, 95–139.

27 N. Ye, Q. Chen, B. Wu and C. Chen, Searching for new nonlinear optical materials on the basis of the anionic group theory, *J. Appl. Phys.*, 1998, **84**, 555–558.

28 H. T. Tian, C. S. Lin, X. Zhao, S. H. Fang, H. Li, C. Wang, N. Ye and M. Luo, Design of a new ultraviolet nonlinear optical material  $\text{KNO}_3\text{SO}_3\text{NH}_3$  exhibiting an unexpected strong second harmonic generation response, *Mater. Today Phys.*, 2022, **28**, 100849.

29 Z. S. Lin, Z. Z. Wang, C. T. Chen and M. H. Lee, Mechanism of linear and nonlinear optical effects of KDP and urea crystals, *J. Chem. Phys.*, 2003, **118**, 2349.

30 P. Yu, L. M. Wu, L. J. Zhou and L. Chen, Deep-Ultraviolet Nonlinear Optical Crystals:  $\text{Ba}_3\text{P}_3\text{O}_{10}\text{X}$  ( $\text{X} = \text{Cl, Br}$ ), *J. Am. Chem. Soc.*, 2014, **136**, 480–487.

31 H. Yu, J. Young, H. Wu, W. Zhang, J. M. Rondinelli and P. S. Halasyamani,  $\text{M}_4\text{Mg}_4(\text{P}_2\text{O}_7)_3$  ( $\text{M} = \text{K, Rb}$ ): Structural Engineering of Pyrophosphates for Nonlinear Optical Applications, *Chem. Mater.*, 2017, **29**, 1845–1855.

32 P. Becker, S. Ahrweiler, P. Held, H. Schneeberger and L. Bohatý, Thermal expansion, pyroelectricity and linear optical properties of  $\text{Li}_2\text{SeO}_4 \cdot \text{H}_2\text{O}$  and  $\text{Li}_2\text{SO}_4 \cdot \text{H}_2\text{O}$ , *Cryst. Res. Technol.*, 2003, **38**, 881–889.

33 C. Wu, X. X. Jiang, Y. L. Hu, C. B. Jiang, T. H. Wu, Z. S. Lin, Z. P. Huang, M. G. Humphrey and C. Zhang, A Lanthanum Ammonium Sulfate Double Salt with a Strong SHG Response and Wide Deep-UV Transparency, *Angew. Chem., Int. Ed.*, 2022, **61**, e202115855.

34 J. Lu, J. N. Yue, L. Xiong, W. K. Zhang, L. Chen and L. M. Wu, Uniform alignment of non- $\pi$ -conjugated species enhances deep ultraviolet optical nonlinearity, *J. Am. Chem. Soc.*, 2019, **141**, 8093–8097.

35 X. Hao, M. Luo, C. S. Lin, G. Peng, F. Xu and N. Ye,  $\text{M}(\text{NH}_2\text{SO}_3)_2$  ( $\text{M} = \text{Sr, Ba}$ ): Two Deep-Ultraviolet Transparent Sulfamates Exhibiting Strong Second Harmonic Generation Responses and Moderate Birefringence, *Angew. Chem., Int. Ed.*, 2020, **60**, 7621–7625.

36 G. Peng, Y. Yang, Y. H. Tang, M. Luo, T. Yan, Y. Q. Zhou, C. S. Lin, Z. S. Lin and N. Ye, Collaborative enhancement from  $\text{Pb}^{2+}$  and  $\text{F}^-$  in  $\text{Pb}_2(\text{NO}_3)_2(\text{H}_2\text{O})\text{F}_2$  generates the largest second harmonic generation effect among nitrates, *Chem. Commun.*, 2017, **53**, 9398–9401.

37 C. Wu, X. X. Jiang, X. J. Wang, Z. S. Lin, Z. P. Huang, X. F. Long, M. G. Humphrey and C. Zhang, Giant optical anisotropy in the UV-transparent 2D nonlinear optical material  $\text{Sc}(\text{IO}_3)_2(\text{NO}_3)$ , *Angew. Chem., Int. Ed.*, 2021, **60**, 3464–3468.

38 J. L. Song, C. L. Hu, X. Xu, F. Kong and J. G. Mao, A Facile Synthetic Route to a New SHG Material with Two Types of Parallel  $\pi$ -Conjugated Planar Triangular Units, *Angew. Chem., Int. Ed.*, 2015, **54**, 3679–3682.

39 Y. Long, X. H. Dong, H. M. Zeng, Z. E. Lin and G. H. Zou, Layered perovskite-like nitrate  $\text{Cs}_2\text{Pb}(\text{NO}_3)_2\text{Br}_2$  as a multifunctional optical material, *Inorg. Chem.*, 2022, **61**, 4184–4192.

40 C. T. Chen, G. L. Wang, X. Y. Wang and Z. Y. Xu, Deep-UV nonlinear optical crystal KBe<sub>2</sub>BO<sub>3</sub>F<sub>2</sub>-discovery, growth, optical properties and applications, *Appl. Phys. B*, 2009, **97**, 9–25.

41 H. T. Tan, C. S. Lin, Y. Q. Zhou, X. Zhao, H. X. Fan, T. Yan, N. Ye and M. Luo, Design of the Ionic Organic Nonlinear Optical Material NH<sub>4</sub>[LiC<sub>3</sub>H(CH<sub>3</sub>)O<sub>4</sub>] with Ultrawide Band Gap and Moderate Birefringence, *Angew. Chem., Int. Ed.*, 2023, e202304858.

42 H. T. Tian, C. S. Lin, B. X. Li, X. Zhao, T. Yan, N. Ye and M. Luo, Designing Strong Polarity and High Configurational Entropy Flexible Units toward Excellent Ultraviolet Nonlinear Optical Materials, *Adv. Funct. Mater.*, 2024, 2402295.